Applied Catalysis B: Environmental 205 (2017) 505–513

Contents lists available at ScienceDirect

Applied Catalysis B: Environmental

journal homepage: www.elsevier.com/locate/apcatb

Highly efficient Pt/$NaNbO_3$ nanowire photocatalyst: Its morphology effect and application in water purification and H_2 production

Qianqian Liu, Yuanyuan Chai, Lu Zhang, Jia Ren, Wei-Lin Dai *

Department of Chemistry and Shanghai Key Laboratory of Molecular Catalysis and Innovative Materials, Fudan University, Shanghai 200433, PR China

ARTICLE INFO

Article history:
Received 18 October 2016
Received in revised form
16 December 2016
Accepted 28 December 2016
Available online 29 December 2016

Keywords:
$NaNbO_3$ nanowire
Pt nanoparticles
Photocatalytic H_2 production
Strong metal-support interaction

ABSTRACT

Pt nanoparticles (NPs) supported on wire- and cube- like $NaNbO_3$ were successfully synthesized by a facile hydrothermal route combined with in situ photodeposition method. Photocatalytic performances towards photocatalytic H_2 production and organic-pollutant degradation of $NaNbO_3$ with morphology of nanowire and nanocube, with or without support of Pt NPs were comparatively investigated. In addition, special attention was paid to investigate the influence of the morphologies on the photocatalytic performance of Pt/$NaNbO_3$ systems. It was found that, by incorporation of Pt NPs, Pt/$NaNbO_3$ systems show much higher activity than their counterparts. Moreover, by contrast with Pt/$NaNbO_3$ nanocube, the Pt NPs tend to be better uniformly dispersed on $NaNbO_3$ nanowire while prefer to agglomerate on $NaNbO_3$ nanocube, resulting in more direct contact between Pt NPs and $NaNbO_3$ nanowire. Meanwhile, it was found that the stronger interaction of Pt NPs and $NaNbO_3$ nanowire, confirmed by XRD, Raman spectroscopy and XPS, significantly enhanced the electron transfer between $NaNbO_3$ nanowire and Pt NPs, and hence further increased the separation efficiency of electron-hole pairs. Thus, a remarkably more enhanced photocatalytic activity of Pt/$NaNbO_3$ nanowire than other materials has been realized, and this catalyst presented super stability as well. A deep insight into the underlying of the photocatalytic reaction mechanism was also proposed.

1. Introduction

Photocatalysis, based on its application in environment purification, waste water treatment, and water photo-splitting, has been regarded as a research focus in the field of environment science [1–4]. Among the promising photocatalysts, perovskite niobates, including $NaNbO_3$, play a noticeable role because of their excellent properties, such as piezoelectric, ferroelectric, ionic conductive and photocatalytic properties [5–10]. Recently, $NaNbO_3$ has been demonstrated as a promising photocatalytic material which can initiate photocatalytic water splitting under UV light irradiation [11]. However, it is usually synthesized by a conventional solid-state reaction or molten salt synthesis routes, which needs very high sintered temperature [12–14]. Therefore, the synthesis of $NaNbO_3$ with controllable structure by hydrothermal process is an effective and attracting attempt because an outstanding advantage of such a hydrothermal method is that the reaction temperature required is much lower than those in other ways. However, the low quantum efficiencies and high band gap (3.0–4.7 eV) of niobates still significantly restrict their practical applications in photocatalysis [15].

In order to improve the photocatalytic activity of niobates, a metal particles (such as Au, Ag and Pt)/semiconductor system has exhibited significant promise. Because on the one hand, the conduction band electrons of semiconductor could be injected into the noble metals with the fermi energy (E_F) lower than the semiconductor conduction band potential through the metal/semiconductor interface, and these electrons are effectively involved in catalysis [16–19]. Yet on the other hand, growth of metals on semiconductors contributes to the improvement of charge separation efficiency of the two materials due to the energy band alignment. Thus, many metal/semiconductor composite photocatalysts have been proposed, such as Ag-$NaTaO_3$ hybid [20], Au loaded $KNbO_3$ [16] and Au loaded TiO_2 [21,22]. Synergistic effects are expected to play a key role in enhancing the photocatalytic performance.

The main focus in the synthesis of metal particles/semiconductor materials is to precisely control the structure of semiconductor [23–26], since the photocatalytic properties are closely related to the morphology and the microstructure of the material [27]. For example, Ruan et al. have reported that the photocatalytic activity of $Bi_2Fe_4O_9$ nanosheets towards the

* Corresponding author.
E-mail address: wldai@fudan.edu.cn (W.-L. Dai).

http://dx.doi.org/10.1016/j.apcatb.2016.12.065
0926-3373/

degradation of methyl orange is higher than that of $Bi_2Fe_4O_9$ microplatelets [28]. However, to date, there are limited studies on the photocatalytic efficiency of metal particles loaded on niobates with disparate morphologies. It is commonly accepted that the morphologies have great influence on their light harvesting ability and activity site number as well as the accessibility to the active sites [29]. Especially, one-dimension (1D) materials, such as nanowire, have gained intensive attention due to their high aspect ratio, quantum refinement effects and much more active sites which are expected to show much higher photocatalytic activities [30,31]. Thus, based on these advantages, the introduction of metal particles in niobates with controllable morphologies would possibly result in significant differences in photocatalytic performance.

In this work, heterostructured Pt/$NaNbO_3$ nanowires and nanocubes were respectively prepared via a simple hydrothermal treatment method combined with the photodeposition. Special attention was paid to investigate the influence of the morphologies on the photocatalytic performance of Pt/$NaNbO_3$ systems. The contrast of synergistic effects between Pt nanoparticles and $NaNbO_3$ nanowire or nanocube was discussed. Their photocatalytic activities were studied for water splitting as well as degrading organic dyes under sunlight irradiation. Additionally, possible mechanism of Pt/$NaNbO_3$ systems in the photocatalytic process were discussed and proposed in detail.

2. Experimental

2.1. Preparation of $NaNbO_3$ and Pt/$NaNbO_3$

2.1.1. $NaNbO_3$ nanowire

Nb_2O_5 (4N, Sinopharm Chemical Reagent Co. Ltd) and NaOH (AR, Sinopharm Chemical Reagent Co. Ltd) were involved in the synthesis. In a typical procedure, 1.0 g of Nb_2O_5 and 10 M NaOH were dissolved in 60 mL of deionized water. After 1 h of magnetic stirring, the obtained mixture was autoclaved at a temperature of 180 °C (hydrothermal reaction) for 2 h to yield white niobate solids. Soon afterwards, the white precipitate was washed with deionized water and pure ethanol several times to remove the residues and then dried at 100 °C overnight. Finally, the product was calcined at 600 °C for12 h.

2.1.2. $NaNbO_3$ nanocube

The procedure was the same as that of $NaNbO_3$ nanowire except that the hydrothermal treatment time was 3 h.

2.1.3. Pt/$NaNbO_3$ nanowire and nanocube

0.3 g of $NaNbO_3$ nanowire or $NaNbO_3$ nanocube were dispersed into 40 mL of deionized water, and 1.6 mL of aqueous $H_2PtCl_6{\cdot}6H_2O$ solution (10 mg/ mL) was added. Then, the resulting suspension was illuminated by 300 W Xe light at room temperature for 4 h under magnetic stirring. Afterwards, the product was filtered and washed several times with deionized water. Finally, the precipitate was dried at 80 °C for 12 h in an oven, and the theoretical Pt loading in the products is 2 wt%. Besides, for Pt/NaNbO3 nanowire, the Pt loading has been adjusted by changing the $H_2PtCl_6{\cdot}6H_2O$ concentration to optimize the best Pt amount.

2.2. Characterization of the catalysts

Scanning electron micrographs (SEM) were obtained using a PHILIPS XL 30 microscope operating at accelerating voltage of 20 kV. TEM images were performed on a JOEL JEM 2010 transmission electron microscope. The samples were supported on carbon-coated copper grids for the experiment. XRD patterns were obtained on a Bruker D8 advance spectrometer with Cu *Kα* radiation (λ = 0.154 nm), operated at 40 mA and 40 kV, respectively. The Laser Raman experiments were performed with a Jobin Yvon Dilor Labram I Raman spectrometer equipped with a holographic notch filter, CCD detector, and He-Ne laser radiating at 632.8 nm. XPS was performed using a RBD 147 upgraded Perkin Elmer PHI 5000C ESCA system equipped with a dual X-ray source, of which the Mg *Kα* (1253.6 eV) anode and a hemispherical energy analyzer was used. The background pressure during data acquisition was maintained at $<10^{-6}$ Pa. Measurements were performed at a pass energy of 93.90 eV. All binding energies were calibrated using contaminant carbon (C 1s = 284.6 eV). Photoluminescence (PL) spectra were carried out on a JASCO FP-6500 type fluorescence spectrophotometer. Electrochemical impedance spectroscopy (EIS) experiment was carried out on a ZENNIUM electrochemical workstation (Zahner, Germany). EIS was conducted in a frequency range of 200 kHz to 5 MHz for 10 mV in DC potential of open circuit potential (OCP) after a 10 min delay. Ultraviolet visible (UV–vis) diffuse reflectance spectra (DRS) spectra were recorded on a SHIMADZU UV-2450 instrument with a collection speed of 40 nm min^{-1} using $BaSO_4$ as the reference.

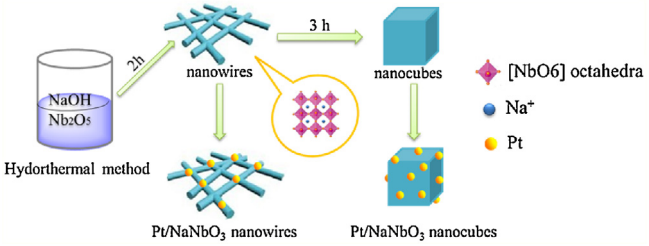

Scheme 1. Schematic flowchart of general procedures for the synthesis of Pt/$NaNbO_3$ nanowire and nanocube.

2.3. Photocatalytic test

Water-splitting reaction was carried out in a top irradiation vessel connected to a glass closed gas circulation system. 100 mg of the photocatalyst was dispersed in 100 mL aqueous solution containing 20% CH_3OH scavenger in volume. The reactant solutions were degassed several times to remove air and then irradiated with a 300 W Xe arc lamp (CeauLight, CEL-HXF300) at room temperature. The amount of H_2 was analyzed by gas chromatograph equipped with a thermal conductivity detector (TCD) and a 5 A molecular sieve column, using Ar as the carrier gas.

Photodegradation experiments were performed in a beaker placed under the lamp bracket, containing reaction solution of RhB or 4-CP (10 mg/L, 100 mL) and 100 mg of catalyst powder. The photo-reactor was equipped with a cooling jacket to maintain the temperature at 25 °C and a 300 W Xe arc lamp (CeauLight, CEL-HXF300). In the experiments, the solution was stirred in dark for 30 min to achieve the adsorption/desorption equilibrium. After turning on the lamp, 5 mL of solution was sampled at certain time intervals and centrifuged for UV–vis absorption spectrum measurements.

3. Results and discussion

3.1. Characterization

$NaNbO_3$, known as one of the perovskite family, contains a network of corner-shared octahedral units of [NbO_6] (as described in Scheme 1) [32–34], which is helpful for the enhancing of charge migration in the crystals. The formation routes of the catalysts were illustrated also in Scheme 1. As shown, the hydrothermal time plays

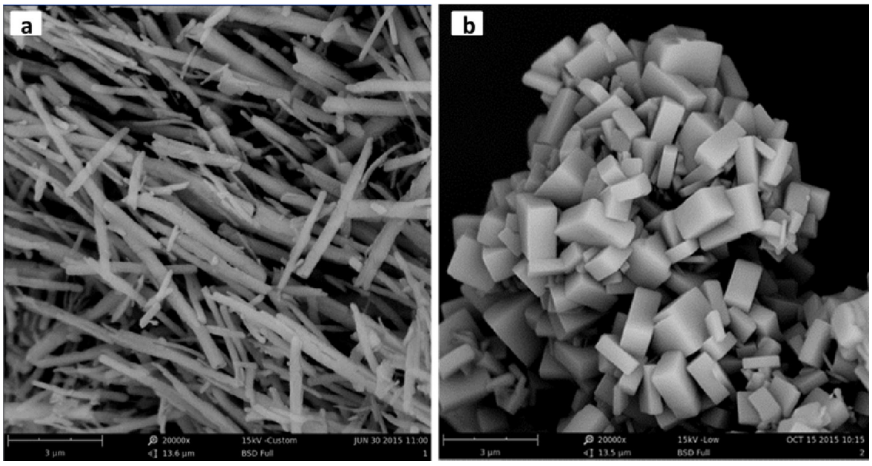

Fig. 1. SEM images of $NaNbO_3$ nanowire (a) and $NaNbO_3$ nanocube (b).

a key role to control $NaNbO_3$ with different morphological characteristics, as $NaNbO_3$ nanocubes are thermodynamically more stable than the crystal of the nanowires [35], and longer reaction time is beneficial for the transformation from $NaNbO_3$ nanowire to $NaNbO_3$ nanocube. Thus, the total transformation of wires to cubes could be observed when the hydrothermal treatment time was extended to 3 h. Finally, after the photo-reduction deposition of Pt NPs, the gray nanocomposites of $Pt/NaNbO_3$ nanowire and $Pt/NaNbO_3$ nanocube were successfully prepared.

The morphology of the $NaNbO_3$ nanowire and $Pt/NaNbO_3$ nanowire were observed by SEM, TEM and HRTEM analyses. The SEM analyses in Fig. 1a and Fig. S1 show a large amount of $NaNbO_3$ nanowires with a uniform diameter of about 100 nm and length of up to several tens micrometers. TEM images (Fig. 2a) reveal that Pt NPs (black spots) are homogeneously dispersed on the surface of $NaNbO_3$ nanowires and their average diameter is 1.2 nm. High-resolution TEM (HRTEM) images (Fig. 2b), taken from the region marked in Fig. 2a, demonstrate both the $NaNbO_3$ nanowires and the Pt NPs are well crystallized, as evidenced by the clear lattice fringes of 0.392, 0.271 and 0.221 nm, which corresponds to the (101), (200) facet of $NaNbO_3$ and (111) facet of Pt NPs, respectively. What's more, a close contact between Pt NPs and $NaNbO_3$ nanowires is observed, which is beneficial for the separation of photo-induced electron-hole pairs. In addition, a selected area electron diffraction (SAED) pattern (inset of Fig. 2b) reveals the $NaNbO_3$ nanowire is of single crystal. And Na, Nb, O and Pt elements clearly emerge in the heterostructures of $Pt/NaNbO_3$ nanowire (seen in X-ray energy dispersive spectroscopy (EDS) elemental mapping (Fig. 2c and d)), indicating the successful combination of Pt NPs with $NaNbO_3$ nanowires. Noticeably, the distribution of all the elements is homogeneous and uniform, which is consistent with the results of TEM (Fig. 2a).

By contrast, the SEM images of $NaNbO_3$ nanocube in Fig. 1b reveal that cube-like $NaNbO_3$ with size ranges from 0.5 to 1.5 μm has been successfully prepared. HRTEM images (Fig. 2f) demonstrate that $NaNbO_3$ nanocubes with (200) crystalline lattices and Pt NPs with (111) crystalline lattices are highly crystallized, and single crystal is also confirmed by SAED pattern (inset of Fig. 2f). In contrast with the $Pt/NaNbO_3$ nanowire, it is noticed that Pt NPs with mean diameter of 1.9 nm prefer to agglomerate on the surface of $NaNbO_3$ nanocubes (Fig. 2e), which would result in less direct contact between Pt NPs and $NaNbO_3$ nanocubes, thus further hindering the separation of electron-hole pairs. In addition, elemental mapping analysis (Fig. S2) further disclosed the inferior dispersion of Pt NPs on the surface of $NaNbO_3$ nanocubes.

Therefore, according to the above comparison and analysis, we found that Pt NPs tend to better disperse on $NaNbO_3$ nanowires while prefer to agglomerate on $NaNbO_3$ nanocubes. The HRTEM images show that $NaNbO_3$ nanowires exhibited two kinds of lattice fringe directions of (101) and (200). While only one kind of lattice fringe directions attributed to (200) planes was observed for the nanocubes, suggesting that the nanocubes just exposed (200) planes. Maybe the high percentage of (101) facets in $NaNbO_3$ nanowires is responsible for their better dispersibility. Just like Ding et al. reported that silver nanoparticles were highly dispersed on the (001) facets of the WO_3-110 support while came to aggregate on the (010) and (100) facets of WO_3 nanorods [36]. It is commonly accepted that a better dispersion of Pt NPs contributes to the more direct contact of Pt NPs and $NaNbO_3$ nanowire, which is beneficial for the absorbance of more sunlight as well as the improvement of light-utilization efficiency of $Pt/NaNbO_3$ nanowire.

Additionally, based on the results of ICP-AES (Table 1), the weight percentages of Pt in 2 wt% $Pt/NaNbO_3$ nanowire and nanocube are measured to be 1.75 and 1.67, which was approximate to the theoretical loadings. However, the surface Pt content calculated from the XPS for $Pt/NaNbO_3$ nanowire is obviously much lower than that of $Pt/NaNbO_3$ nanocube. Given the determined bulk percentage of Pt, we found that the Pt NPs tend to penetrate into the lattice of $NaNbO_3$ nanowire, while prefer to appear on the surface of $NaNbO_3$ nanocube.

In order to verify the above speculation, XRD technique was carried out. As shown in Fig. 3, the characteristic diffraction peaks of $NaNbO_3$ nanowire (Fig. 3d) and $NaNbO_3$ nanocube (Fig. 3b) match well with the standard card of orthorhombic phase (JCPDS 33-1270). However, no signal of metallic Pt phase can be detected in $Pt\text{-}NaNbO_3$ systems because of the small crystallite size and low Pt content. Moreover, by comparing with pure $NaNbO_3$ nanowire, slight characteristic diffraction peak shifts of $Pt/NaNbO_3$ nanowire are observed (inset of Fig. 3), indicating that Pt NPs incorporate into the lattice of $NaNbO_3$ nanowire. The lattice parameter calculated by Rietveld refinement of the XRD data shows that, for $Pt/NaNbO_3$ nanowire, this value becomes smaller in (100) and (010) directions, but increases in (001) compared to that of pristine $NaNbO_3$ (Table 2), indicating the lattice shrinkage induced by Pt incorporated into the lattice of $NaNbO_3$ nanowire. Meanwhile, by contrast, no diffraction pattern shifts can be seen in $Pt/NaNbO_3$ nanocube, suggesting very few Pt NPs penetrate into the lattice of $NaNbO_3$ nanocube, which is consistent with the results in Table 1. On the other hand, the observed shifts demonstrate the strong interaction between Pt NPs and $NaNbO_3$ nanowire. It is known that strong metal-support interaction may promote electron trans-

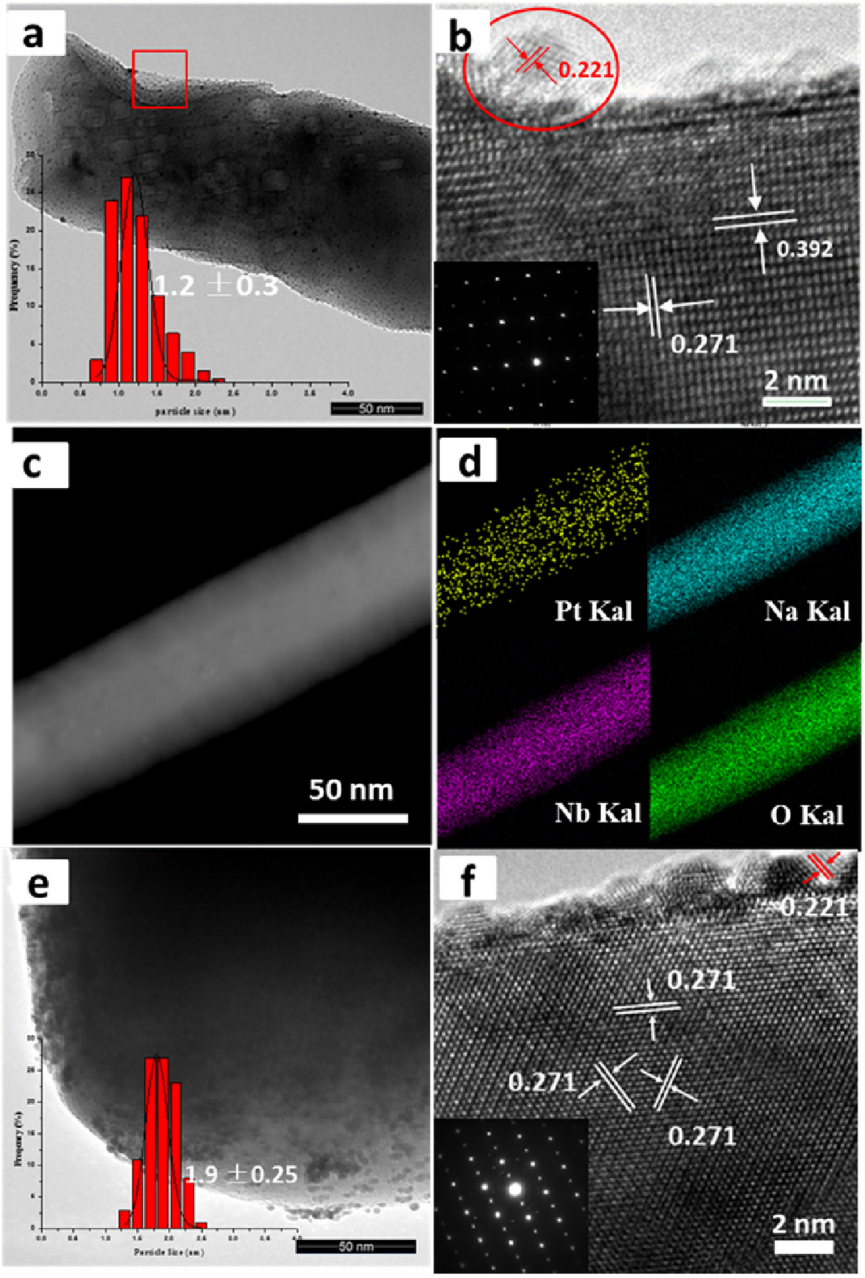

Fig. 2. TEM image of Pt/$NaNbO_3$ nanowire (a) and size distribution of the Pt particles (inset). HRTEM image of Pt/$NaNbO_3$ nanowire (b) and inset of a SAED pattern. Dark-field TEM image of Pt/$NaNbO_3$ nanowire and the corresponding elemental area mapping results (c, d). TEM image of Pt/$NaNbO_3$ nanocube (e) and size distribution of the Pt particles (inset). HRTEM image of Pt/$NaNbO_3$ nanocube (f) and inset of a SAED pattern.

Table 1
The surface composition and atomic ratios of different catalysts.

Catalyst	Surface Composition (%)				Surface atomic ratio		
	Na	Nb	O	Pt	Pt/Nb[a]	Pt/Nb[b]	Pt content (wt%)[b]
$NaNbO_3$ nanowire	2.08	3.08	23.42	–	–	–	–
Pt/$NaNbO_3$ nanowire	2.07	5.71	29.59	0.23	0.022	0.015	1.75
$NaNbO_3$ nanocube	4.34	4.97	29.09	–	–	–	–
Pt/$NaNbO_3$ nanocube	1.66	4.52	27.59	1.98	0.438	0.014	1.67

[a] Determined by XPS.
[b] Determined by ICP.

fer and further enhance the separation of electron-hole pairs, thus contributing to the enhancement of photoactivity over Pt/$NaNbO_3$ nanowire [37–40]. However, no shifts in XRD pattern of Pt/$NaNbO_3$ nanocube may result from the weaker metal-support interaction between Pt NPs and $NaNbO_3$ nanocube.

Raman spectroscopy, known as an appropriate technique for the investigation of the short-range order, phase structure and space

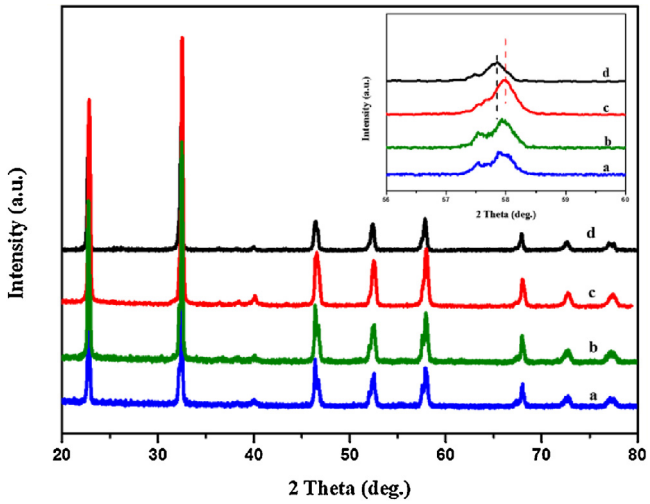

Fig. 3. XRD patterns of (a) Pt/$NaNbO_3$ nanocube, (b) $NaNbO_3$ nanocube, (c) Pt/$NaNbO_3$ nanowire and (d) $NaNbO_3$ nanowire.

Table 2
Lattice parameter of niobate samples.

Samples	Lattice parameter		
	a (Å)	b (Å)	c (Å)
$NaNbO_3$ nanowire	5.549	15.558	5.507
Pt/$NaNbO_3$ nanowire	5.528	15.484	5.515

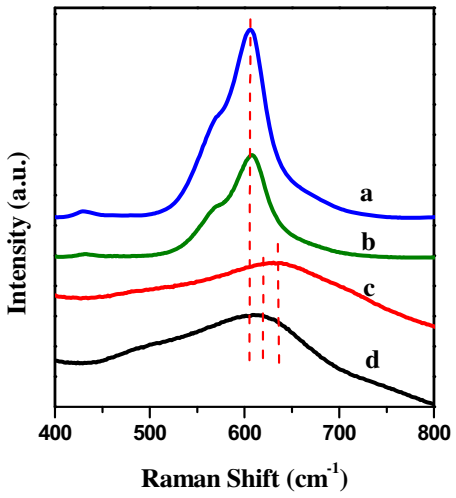

Fig. 4. Raman spectroscopy of (a) $NaNbO_3$ nanocube, (b) $NaNbO_3$ nanowire, (c) Pt/$NaNbO_3$ nanowire, and (d) Pt/$NaNbO_3$ nanocube.

group in perovskites, is employed to further analyze the crystalline phase of the as-prepared products. As shown in Fig. 4, the strongest band near 600 cm^{-1} corresponds to the stretching model of Nb—O octahedron. After Pt NPs incorporates, the characteristic band shifts to higher wavenumber and is remarkably broadened (Fig. 4c and d). The observed shift and broadening can be assigned to the incorporation of Pt NPs into the lattice of $NaNbO_3$, which is consistent with the XRD result. Clearly, the shift of Pt/$NaNbO_3$ nanowire is much higher than Pt/$NaNbO_3$ nanocube, further illustrating the interaction of the former is much stronger than the latter. On the other hand, it is known that the Raman shifts for stretching is closely related to the Nb-O bond lengths in crystalline inorganic niobate compounds. And the higher wavenumber for the Raman stretching bands corresponds to shorter Nb-O bond lengths [41–44]. Thus, the observed shifts in Fig. 4 can be ascribed to the changes of Nb-O bond lengths. It has been reported that the O 2p and Nb 4d orbital mainly contribute to the formation of the valence and conduction bands of $NaNbO_3$ [45]. Therefore, the changes in the NbO_6 octahedra local structure, such as Nb-O bond lengths, may influence on the band structure of the $NaNbO_3$, and thus resulted in the variation of the optical band gap, which would be discussed in the mechanism part.

To further investigate the chemical state of the as-prepared samples, XPS measurements were carried out and the results were shown in Fig. 5. From Fig. 5a, the Pt 4f spectrum can be deconvoluted into two peaks centered at around 70.7 eV (Pt $4f_{7/2}$) and 74.1 eV (Pt $4f_{5/2}$), which is the characteristic of metallic platinum, indicating that metallic platinum is formed in the product. Simultaneously, the Nb 3d spectra of $NaNbO_3$ nanowire in Fig. 5b displays two signals at 207.8 eV (Nb $3d_{5/2}$) and 210.5 eV (Nb $3d3_{/2}$), suggesting that Nb is in the Nb (+5) chemical state. Compared to those of the pristine $NaNbO_3$ nanowire, the Nb 3d peaks of Pt/$NaNbO_3$ nanowire migrate to the direction of lower binding energy, indicating the presence of Pt NPs strongly interacts with $NaNbO_3$ nanowire, which greatly facilitates the electrons transfer. Additionally, based on the report of Zhou et al. the reduction of Nb^{5+} can actually harvest the light energy more efficiently and this will be beneficial for the improvement of photocatalytic performance [46]. Whereas, as a contrast, the Pt 4f spectrum of Pt/$NaNbO_3$ nanocube (Fig. 5c) can be split into four peaks. The binding energies of 70.6 and 74.0 eV are attributed to Pt $4f_{7/2}$ and Pt $4f_{5/2}$ of Pt metal, while the other peaks at approximate 73.3 and 76.7 eV are attributed to the platinum oxide layer, which covered the surface of Pt metal particles. The appearance of platinum oxide peaks apparently indicates Pt NPs are located on the surface of Pt/$NaNbO_3$ nanocube. Consistently, in contrast with Pt/$NaNbO_3$ nanowire, less peak shifts are observed in Nb^{5+} of Pt/$NaNbO_3$ nanocube (Fig. 5d), further demonstrating the interaction between Pt and $NaNbO_3$ nanowire is more stronger than that of Pt/$NaNbO_3$ nanocube. This finding is consistent with the results of XRD and Raman spectroscopy.

3.2. Photocatalytic tests

The photocatalytic activities of the different samples were firstly estimated by the photocatalytic hydrogen evolution under mimic sunlight irradiation. As shown in Fig. 6a and b, a tremendously enhanced H_2 evolution rate of 26.6 μmol h^{-1} is achieved on Pt/$NaNbO_3$ nanowire, which is about 24 times and 8.3 times higher than that of Pt/$NaNbO_3$ nanocube (1.1 μmol h^{-1}) and pure $NaNbO_3$ nanowire (3.2 μmol h^{-1}), respectively. While $NaNbO_3$ nanocube exhibits negligible activity (0.5 μmol h^{-1}), ulteriorly manifesting the stronger interaction between Pt NPs and $NaNbO_3$ nanowire (confirmed by the results from XRD, Raman spectroscopy and XPS) is beneficial for the separation of electron-hole pairs, and hence further contributes to the enhancement of photoactivity.

Additionally, the catalytic performance comparison of Pt/$NaNbO_3$ nanowire in this work with the state-of-the-art record concerning $NaNbO_3$ is shown in Table S1. As can be seen, the hydrogen production varies depending on different factors, including the reaction conditions, the mass of catalysts, nature of the support, irradiation wavelength, and others. A clear comparison of the results reported in the literatures is very difficult because of the obvious differences in the reaction processes. However, in the catalysts studied in this work, it is important to highlight the large amount of hydrogen produced under the same of reaction conditions, compared to previous works. The quantum yield was measured as about 0.53%, which was calculated using the formula listed in supporting information.

Except for the superior photocatalytic hydrogen production capacity of Pt/$NaNbO_3$ nanowire, as demonstrated above, the photocatalytic aqueous-phase oxidations of RhB and 4-CP were also

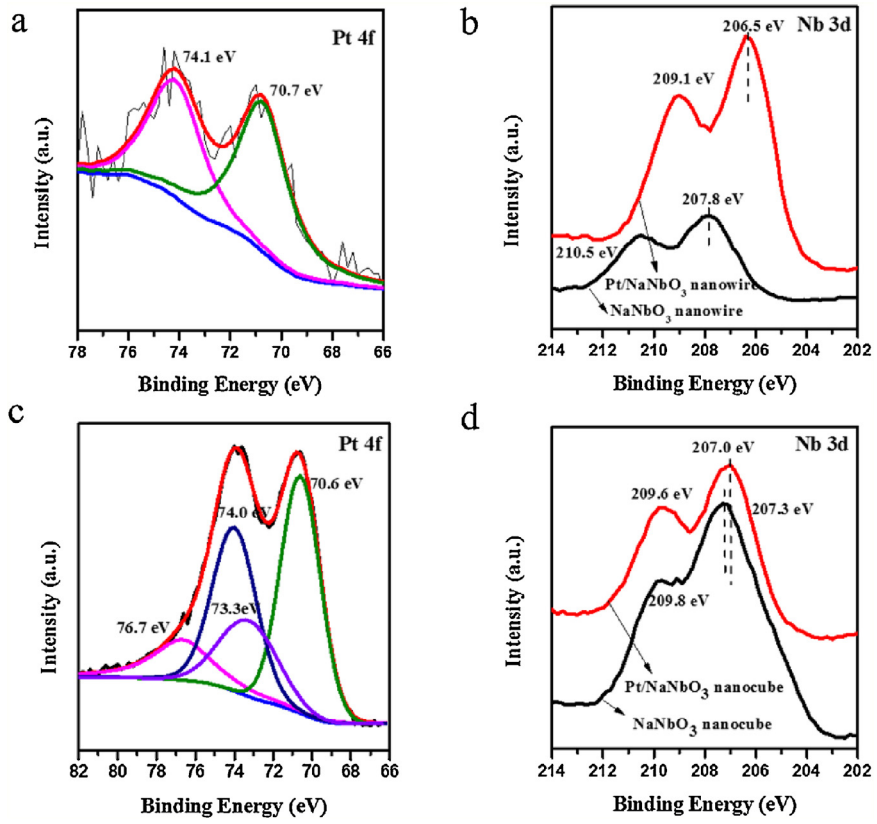

Fig. 5. XPS spectra of $Pt/NaNbO_3$ nanowire in the Pt 4f (a), Nb 3d (b) regions and $Pt/NaNbO_3$ nanocube in the Pt 4f (c), Nb 3d (d) regions.

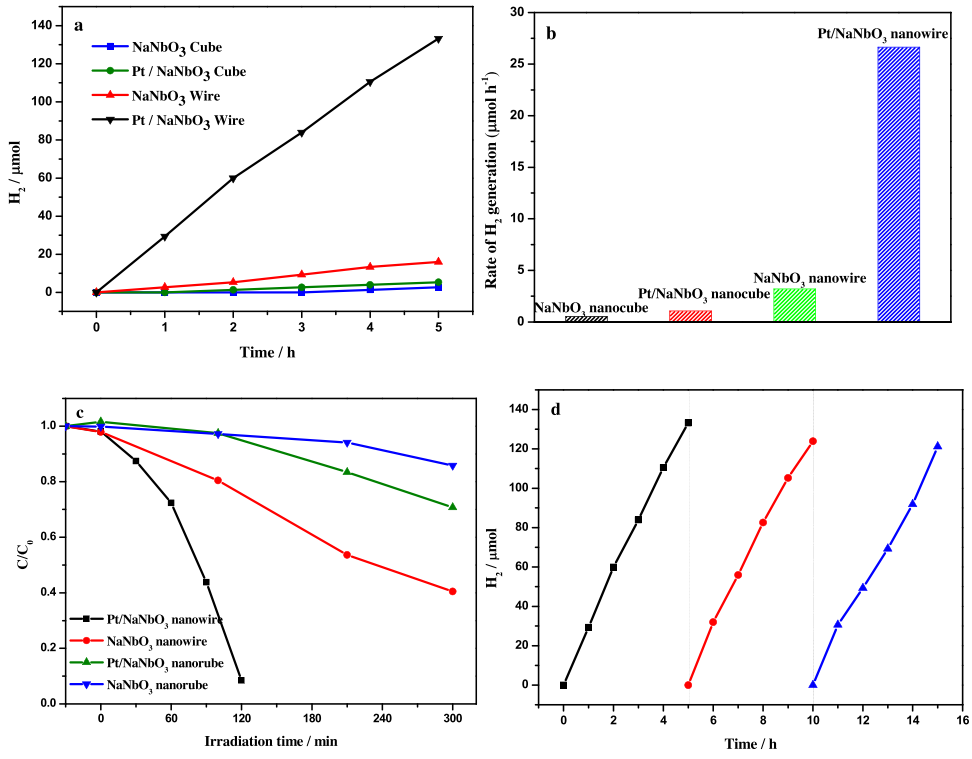

Fig. 6. Photocatalytic H_2 generation under sunlight irradiation (a) and the H_2 generation rates of various photocatalysts (b); photoactivity for the degradation of RhB over different photocatalysts under sunlight irradiation (c); reusability of $Pt/NaNbO_3$ nanowire for the photocatalytic H_2 production under sunlight irradiation (d).

examined. As shown in Fig. 6c, dark absorption of RhB for 30 min reveals that the self-photolysis of RhB is negligible, and no adsorption phenomenon is observed in pure $NaNbO_3$ and $Pt/NaNbO_3$ systems. However, $Pt/NaNbO_3$ nanowire presents appreciably

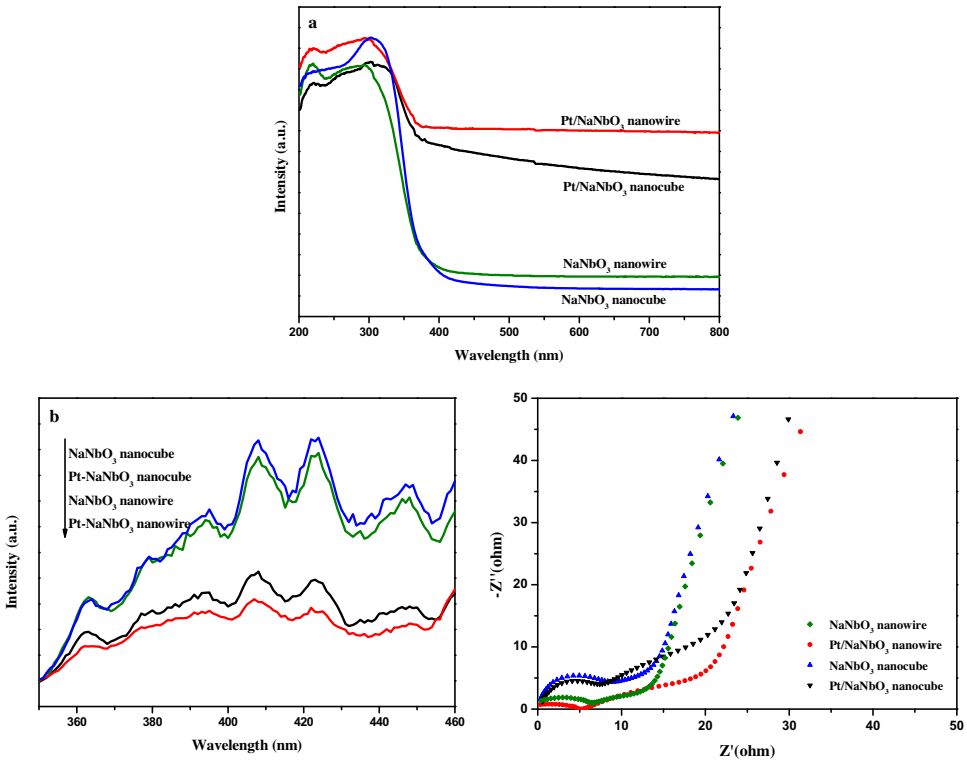

Fig. 7. UV–vis diffuse-reflectance spectra (a), photoluminescence emission spectra of different samples (b), and electrochemical impedance spectra (c) of different photocatalysts.

much higher photocatalytic efficiency than pure $NaNbO_3$ nanowire and Pt/$NaNbO_3$ nanocube, while $NaNbO_3$ nanocube exhibits even negligible activity. The trends are consistent with the photocatalytic hydrogen production. The apparent first-order-rate constant (k) for the photocatalytic degradation RhB is calculated based on a simplified Langmuir-Hinshelwood model (see Fig. S4a) [47]. It clearly demonstrates that the average reaction rate of Pt/$NaNbO_3$ nanowire, about 0.025 min^{-1}, is much higher than that of pure $NaNbO_3$ nanowire (0.003 min^{-1}), Pt/$NaNbO_3$ nanocube (0.001 min^{-1}) and $NaNbO_3$ nanocube (0.00016 min^{-1}). Additionally, the photocatalytic degradation of 4-CP shows similar trends (Fig. S4b). Therefore, it can be concluded that Pt/$NaNbO_3$ nanowire possesses dramatically enhanced activity in the photocatalytic hydrogen production as well as the decomposition of various pollutants.

Moreover, in order to explore the influence of Pt amount, the activity of Pt/$NaNbO_3$ nanowire with different Pt loadings over the degradation of RhB is shown in Fig. S4c. The photocatalytic efficiency increases remarkably with the enhancement of Pt loadings, among which the Pt/$NaNbO_3$ nanowire–2 wt% composite exhibits the optimal photocatalytic activity, approximately 8 times as high as that of pure $NaNbO_3$ nanowire. However, the further increase of Pt NPs amount would lead to the decrease of photocatalytic activity. This result may be due to the higher Pt loadings that lead to the aggregation of the Pt NPs, thus limiting the transfer of photogenerated charge carriers.

Generally, the long-term stability of a photocatalyst is of great significance for its further practical application. Thus, the catalytic stability of Pt/$NaNbO_3$ nanowire was investigated under a prolonged photo-irradiation time up to 15 h in the process of photocatalytic H_2 production. As shown in Fig. 6d, the activity of Pt/$NaNbO_3$ nanowire is still retained over more than 90% of its original activity after three successive experimental runs, meaning the high stability against photocorrosion during photocatalytic H_2 production reaction. In addition, its sufficient stability was further confirmed by the degradation of RhB, as shown in Fig. S4d, and the photocatalytic degradation efficiency of RhB is still higher than 90% even after 5 repeated runs.

3.3. The mechanism of the enhanced photocatalytic activity

In general, the good light absorption capability and high separation efficiency of electron-hole pairs are beneficial for the performance of a photocatalyst [48]. As shown in Fig. 7a, the UV–vis DRS reveals that both bare $NaNbO_3$ nanowire and nanocube only absorb light at λ <400 nm, corresponding to the charge transfer from O 2p (VB) to Nb 4d orbitals (CB). The slight difference of UV–vis DRS spectra is ascribed to their different morphology and size. After deposition of Pt NPs, the Pt/$NaNbO_3$ samples exhibit noticeable red shifts compared with pure $NaNbO_3$, indicating the smaller band gap and better light adsorption performance of Pt/$NaNbO_3$ systems. Meanwhile, the red shifts of Pt/$NaNbO_3$ systems are possibly ascribed to the metal-support interaction, which has been confirmed by XRD, Raman spectroscopy and XPS.

Actually, except for the optical absorption, the efficient charge separation of a photocatalyst always plays a crucial role in determining its photocatalytic property. As illustrated by XPS, most of Pt NPs disperse in the interior of $NaNbO_3$ nanowire but exterior of $NaNbO_3$ nanocube, possibly resulting in the stronger interaction between Pt NPs and $NaNbO_3$ nanowire, which will in turn significantly increase the charge separation of Pt/$NaNbO_3$ nanowire than that of Pt/$NaNbO_3$ nanocube. Moreover, as confirmed by the TEM images, Pt NPs have more uniform distribution on $NaNbO_3$ nanowire with less agglomeration than $NaNbO_3$ nanocube. This difference would contribute to more direct contact between Pt NPs and $NaNbO_3$ nanowire, which may further enhance the separation and transportation efficiency of electron-hole pairs.

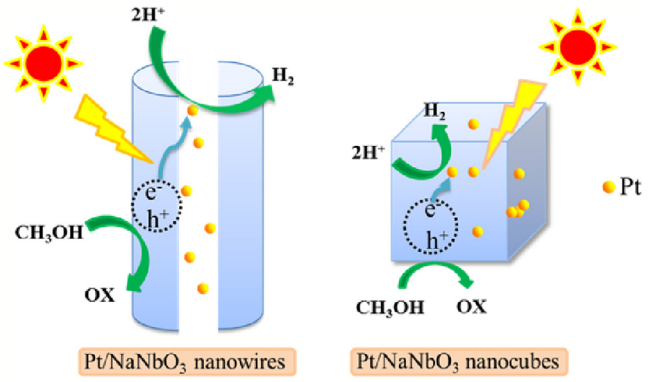

Scheme 2. Schematic illustration of the charge separation and transformation in the $Pt/NaNbO_3$ nanowire and $Pt/NaNbO_3$ nanocube during photocatalytic H_2 production under sunlight irradiation.

PL spectroscopy has been investigated to verify the separation efficiency of the photoinduced charge carriers. As demonstrated in Fig. 7b, all the samples exhibit similar emission profiles under the excitation wavelength at 300 nm. The emission peaks at about 408 and 423 nm in the PL spectra for all samples mainly originate from the localized states and defects of $NaNbO_3$, which has been confirmed by the results of previous work [49,50]. Remarkably, the PL intensity of $Pt/NaNbO_3$ systems is much lower than pure $NaNbO_3$ samples, indicating the $Pt/NaNbO_3$ systems have relative low recombination of electrons and holes. In contrast, the intensity of $Pt/NaNbO_3$ nanowire significantly decreases than that of $Pt/NaNbO_3$ nanocube, corresponding to the higher efficiency of charge separation of $Pt/NaNbO_3$ nanowire, which is coincidence with the above assumption.

EIS analysis is a powerful technique to evaluate the interfacial properties between the electrode and the electrolyte, such as conductivity, structure, and charge transport. The semicircle in the EIS Nyquist plot in the middle frequency region is ascribed to the charge-transfer resistance (R_{ct}) along with double-layer capacitance (CPE) [51,52]. It is generally accepted that the smaller the diameter of semicircle arc of the EIS spectrum is, the lower R_{ct} is, corresponding to more efficient separation of photoexcited electron-holes pairs. Fig. 7c shows the Nyquist plots of as-prepared photocatalysts. Obviously, $Pt/NaNbO_3$ nanowire exhibits the lowest semicircle radius in all samples, further implying that the loading of Pt NPs significantly enhanced the electron migration, thus reducing the recombination of electron–hole pairs.

Based on the experimental results above, a possible photocatalytic reaction mechanism was proposed and briefly described in Scheme 2. Under the mimic sunlight irradiation, photons can be absorbed by $NaNbO_3$ nanowire and cube, which subsequently produce photogenerated electrons and holes. After Pt NPs loading, photogenerated electrons effectively transfer to Pt NPs, and promote the separation of photogenerated electron-hole pairs, which are beneficial for the enhancement of photocatalytic activity. Subsequently, the electrons accumulated on Pt NPs reduce protons to hydrogen, and the photoinduced holes will react with methanol (sacrificial reagent) to reduce the electron-hole recombination. More importantly, it should be noticed that, as compared to $Pt/NaNbO_3$ nanocube, the photocatalytic performance of $Pt/NaNbO_3$ nanowire is significantly enhanced. The enhancement could be attributed to the following factors. (i) Much stronger metal-support interaction between Pt and $NaNbO_3$ nanowire facilitates the charge transfer process. (ii) More uniform dispersion of Pt NPs on $NaNbO_3$ nanowire contributes to better direct contact between them, and hence further improves the separation of electron-hole pairs. (iii) The perfect 1D nanowire morphology exhibits enhanced light harvesting ability and easier accessibility to the active sites compared to $Pt/NaNbO_3$ nanocube.

4. Conclusion

In summary, we have successfully synthesized $Pt/NaNbO_3$ nanowire and $Pt/NaNbO_3$ nanocube through a simple hydrothermal as well as photo-deposition method. Comparative studies were carried out to evaluate the relevant photocatalytic performance of $NaNbO_3$ nanowire, $NaNbO_3$ nanocube, $Pt/NaNbO_3$ nanowire and $Pt/NaNbO_3$ nanocube. It was found that, after incorporation of Pt NPs, the $Pt/NaNbO_3$ systems exhibited noticeably higher performance over their counterparts due to the better light absorption and the improved separation capability of photogenerated electron-hole pairs. More importantly, as compared to $Pt/NaNbO_3$ nanocube, the Pt NPs presented better uniform distribution on $NaNbO_3$ nanowire while prefer to agglomerate on $NaNbO_3$ nanocube, contributing to more direct contact of Pt NPs and $NaNbO_3$ nanowire. In addition, stronger Pt-$NaNbO_3$ nanowire interaction than $Pt/NaNbO_3$ nanocube significantly facilitated the electrons transfer and increased the separation of electron-hole pairs. Thus, a remarkably enhanced photocatalytic activity for hydrogen production and organics degradation of $Pt/NaNbO_3$ nanowire has been demonstrated, which shows good stability as well. Hence, this work provided a promising practical protocatalyst for photocatalytic water splitting as well as organic pollutant degradation. This composite is also of great interest for solar cells, photonic and optoelectronic devices and sensors. Further in-depth studies of the material with different potential applications are being under way.

Acknowledgments

We would like to thank financial support by NSFC (Project 21373054, 21173052), and the Natural Science Foundation of Shanghai Science and Technology Committee (08DZ2270500).

Appendix A. Supplementary data

Supplementary data associated with this article can be found, in the online version, at http://dx.doi.org/10.1016/j.apcatb.2016.12.065.

References

[1] S.F. Chen, Y.F. Hu, S.G. Meng, X.L. Fu, Appl. Catal. B: Environ. 150–151 (2014) 564–573.
[2] G. Liu, p. Niu, C.H. Sun, S.C. Smith, Z.G. Chen, G.Q. Lu, H.M. Cheng, J. Am. Chem. Soc. 132 (2010) 11642–11648.
[3] Q. Xing, J.G. Yu, M. Jaroniec, J. Am. Chem. Soc. 134 (2012) 6575–6578.
[4] Q. Liu, J. Ding, Y. Chai, W.L. Dai, J. Environ. Chem. Eng. 3 (2015) 1072–1080.
[5] Q.P. Ding, Y.P. Yuan, X. Xiong, R.P. Li, H.B. Huang, Z.S. Li, T. Yu, Z.G. Zou, S.G. Yang, J. Phys. Chem. C 112 (2008) 18846–18848.
[6] G.Q. Li, N. Yang, W.L. Wang, W.F. Zhang, J. Phys. Chem. C. 113 (2009) 14829–14833.
[7] Z. Cheng, K. Ozawa, M. Osada, A. Miyazaki, H. Kimura, J. Am. Ceram. Soc. 89 (2006) 1188–1192.
[8] Y. Guo, K. Kakimoto, H. Ohsato, Appl. Phys. Lett. 85 (2004) 4121–4123.
[9] F. Dutto, C. Raillon, K. Schenk, A. Radenovic, Nano Lett. 11 (2011) 2517–2521.
[10] S. Kim, J.H. Lee, J. Lee, S.W. Kim, M.H. Kim, S. Park, H. Chung, Y.I. Kim, W. Kim, J. Am. Chem. Soc. 135 (2013) 6–9.
[11] L.Q. Jiang, Y. Qiu, Z.G. Yi, J. Mater. Chem. A 1 (2013) 2878–2885.
[12] H.F. Shi, G.Q. Chen, Z.G. Zou, Appl. Catal. B: Environ. 156–157 (2014) 378–384.
[13] F. Madaro, R. Sæterli, J.R. Tolchard, M.A. Einarsrud, R. Holmestad, T. Grande, CrystEngComm 13 (2011) 1304–1313.
[14] L.H. Li, J.X. Deng, J. Chen, X.Y. Sun, R.B. Yu, G.R. Liu, X.R. Xing, Chem. Mater. 21 (2009) 1207–1213.
[15] D.B. Xu, S.B. Yang, Y. Jin, M. Chen, W.Q. Fan, B.F. Luo, W.D. Shi, Langmuir 31 (2015) 9694–9699.
[16] L.S. Yan, T.T. Zhang, W.Y. Lei, Q.L. Xu, X.M. Zhou, P. Xu, Y.S. Wang, G. Liu, Catal. Today 224 (2014) 140–146.
[17] M.V. Dozzi, L. Prati, P. Canton, E. Selli, Phys. Chem. Chem. Phys. 11 (2009) 7171.

[18] T. Kiyonaga, Q.L. Jin, H. Kobayashi, H. Tada, ChemPhysChem 10 (2009) 2935.
[19] S. Naya, M. Teranishi, K. Kimura, H. Tada, Chem. Commun. 47 (2011) 3230.
[20] D.B. Xu, M. Chen, S.Y. Song, D.L. Jiang, W.Q. Fan, W.D. Shi, Cryst. Eng. Comm. 16 (2014) 1384–1388.
[21] J. Fang, S.W. Cao, Z. Wang, M.M. Shahjamali, S.C.J. Loo, J. Barber, C. Xue, Int. J. Hydrogen Energy 37 (2012) 17853–17861.
[22] Z. Liu, W. Hou, P. Pavaskar, M. Aykol, S.B. Cronin, Nano Lett. 11 (2011) 1111–1116.
[23] E. Kowalska, O.O.P. Mahaney, R. Abe, B. Ohtani, Phys. Chem. Chem. Phys. 12 (2010) 2344–2355.
[24] Y. Nishijima, K. Ueno, Y. Yokota, K. Murakoshi, H. Misawa, J. Phys. Chem. Lett. 1 (2010) 2031–2036.
[25] D.B. Ingram, P. Christopher, J.L. Bauer, S. Linic, ACS Catal. 1 (2011) 1441–1447.
[26] Z.F. Bian, T. Tachikawa, P. Zhang, M. Fujitsuka, T. Majima, J. Am. Chem. Soc. 136 (2014) 458–465.
[27] D.Q. Zhang, J.Y. Cheng, F. Shi, Z.J. Cheng, X.Y. Yang, M.S. Cao, RSC Adv. 5 (2015) 33001–33007.
[28] Q.J. Ruan, W.D. Zhang, J. Phys. Chem. C 113 (2009) 4168–4173.
[29] X. Jing, T. Wang, Environ. Sci. Technol. 41 (2007) 4441–4446.
[30] Y.Q. Wang, Z.J. Zhang, Y. Zhu, Z.C. Li, R. Vajtai, P.M. Ajayan, ACS Nano 2 (2008) 1492–1496.
[31] Q.L. Gu, K.J. Zhu, N.S. Zhang, Q.M. Sun, P.C. Liu, J.S. Liu, J. Wang, Z.S. Li, J. Phys. Chem. C 119 (2015) 25956–25964.
[32] H.F. Shi, G.Q. Chen, C.L. Zhang, Z.G. Zou, ACS Catal. 4 (2014) 3637–3643.
[33] H.F. Shi, X.K. Li, D.F. Wang, Y.P. Yuan, Z.G. Zou, J.H. Ye, Catal. Lett. 132 (2009) 205–212.
[34] K. Saito, A. Kudo, Inorg. Chem. 49 (2010) 2017–2019.
[35] H.Y. Zhu, Z.F. Zheng, X.P. Gao, Y.N. Huang, Z.M. Yan, J. Zou, H.M. Yin, Q.D. Zou, S.H. Kable, J.C. Zhao, Y.F. Xi, W.N. Martens, R.L. Frost, J. Am. Chem. Soc. 128 (2006) 2373–2384.
[36] J. Ding, Y. Chai, Q. Liu, X. Liu, J. Ren, W.L. Dai, J. Phys. Chem. C 120 (2016) 4345–4353.
[37] J.A. Horsley, J. Am. Chem. Soc. 101 (1979) 2870–2874.
[38] B.A. Sexton, A.E. Hughes, K. Foger, J. Catal. 77 (1982) 85–93.
[39] Y. Shiraishi, Y. Kofuji, S. Kanazawa, H. Sakamoto, S. Ichikawa, S. Tanaka, T. Hirai, Chem. Commun. 50 (2014) 15255–15258.
[40] H. Sakamoto, T. Ohara, N. Yasumoto, Y. Shiraishi, S. Ichikawa, S. Tanaka, T. Hirai, J. Am. Chem. Soc. 137 (1979) 9324–9332.
[41] K. Maeda, T.E. Mallouk, J. Mater. Chem. 19 (2009) 4813.
[42] H.W. Eng, P.W. Barnes, B.M. Auer, P.M. Woodward, J. Solid State Chem. 175 (2003) 94–109.
[43] H. Kato, A. Kudo, Catal. Today 78 (2003) 561–569.
[44] J. Wang, Z. Zou, J. Ye, J. Phys. Chem. Solids 66 (2005) 349–355.
[45] S. Park, H.J. Song, C.W. Lee, S.W. Hwang, I.S. Cho, ACS Appl. Mater. Interfaces 7 (2015) 21860–21867.
[46] C. Zhou, Y. Zhao, L. Shang, Y. Cao, L.Z. Wu, C.H. Tung, T. Zhang, Chem. Commun. 50 (2014) 9554–9556.
[47] Z. Bian, T. Tachikawa, T. Majima, J. Phys. Chem. Lett. 3 (2012) 1422–1427.
[48] Y. Chai, J. Ding, L. Wang, Q. Liu, J. Ren, W.L. Dai, Appl. Catal. B: Environ. 179 (2015) 29–36.
[49] S. Rahimnejad, J.H. He, W. Chen, K. Wu, G.Q. Xu, RSC Adv. 4 (2014) 62423–62429.
[50] S.F. Chen, L. Ji, W.M. Tang, X.L. Fu, Dalton Trans. 42 (2013) 10759–10768.
[51] W.H. Yang, J.M. Wang, T. Pan, J.J. Xu, J.Q. Zhang, C.N. Cao, Chem. Commun. 4 (2002) 710–715.
[52] Y.P. Zhu, T.Z. Ren, Y.P. Liu, Z.Y. Yuan, RSC Adv. 4 (2014) 31754–31758.